Title

CrAlON CAE-PVD coatings for oxidation and wear protection of TZM alloys in FAST sintering applications

Author names and affiliations

Eluxka Almandoz[*a], Jonathan Fernández de Ara[a], Javier Martínez de Bujanda[a,b], José Fernández Palacio[a], Rafael José Rodríguez[c,d], Zhenxue Zhang[e], Hanshan Dong[e], Yi Qin[f], Gonzalo García Fuentes[a].

[a]*Asociación de la Industria Navarra, Carretera Pamplona 1, 31191 Cordovilla, Spain.*

[b]*Escuela Técnica Superior de Ingeniería, Universidad del País Vasco, Alameda Urquijo s/n, 48013 Bilbao, Spain.*

[c]*Universidad Pública de Navarra, Campus de Arrosadía s/n, 31006, Pamplona, Spain.*

[d]*Institute for Advanced Materials - INAMAT, Campus de Arrosadía s/n, 31006, Pamplona, Spain.*

[e]*School of Metallurgy and Materials, University of Birmingham, Birmingham B15 2TT, UK.*

[f]*Department of Design, Manufacturing and Engineering Management, Strathclyde University, Glasgow, G1 1XJ, UK.*

Corresponding author: Eluxka Almandoz - ealmandoz@ain.es

Jonathan Fernández de Ara – jfernandez@ain.es

Javier Martínez de Bujanda – jmbujanda@ain.es

José Fernández Palacio – jfpalacio@ain.es

Rafael José Rodríguez – rafael.rodriguez@unavarra.es

Zhenxue Zhang – Z.Zhang.1@bham.ac.uk

Hanshan Dong – H.DONG.20@bham.ac.uk

Yi Qin – qin.yi@strath.ac.uk

Gonzalo García Fuentes – gfuentes@ain.es

Abstract

In this work CrAlO and CrAlO/CrAlN multilayers deposited by cathodic arc evaporation are evaluated as protective films in metal and ceramic powder FAST sintering tool dies fabricated in titanium-zirconium-molybdenum allows (TZM). The films have been characterised in terms of their composition, microstructure, mechanical properties and thermal stability in air at high temperatures between 800 ºC and 1100 ºC; in addition the tribological performance has been analysed at room temperature and at 400 ºC.

The crystalline structure and composition of the CrAlO based coatings are compatible with the formation of a mixture of α-corundum and a cubic fcc $(Cr,Al)_2O_3$. The crystalline structure of the multilayer is, on the other hand, dominated by the cubic fcc lattice plane reflections of the CrAlN.

The deposited specimens have high hardness, between 25 and 30 GPa, which are stable even after annealing at 1000 ºC. Even more, the multilayer coating also exhibited good mechanical stability at 1100 ºC. The multilayer coating also exhibited an excellent behaviour against wear at 400 ºC.

Sintering trials using coated TZM dies have been carried out using Ti90Sn10 and Al_2O_3 high energy ball milled powders. The experimental results show that the oxide based coating formulations are potentially able to protect the tools from wear, sticking and oxidation of their surfaces. This may allow the use of TZM material as an alternative to other substrates such as graphite.

Keywords

Cathodic arc evaporation; oxide coating; wear resistance; hardness; sintering.

Main text

1. Introduction

Titanium-Zirconium-Molybdenum alloys (TZM) have excellent strength and creep resistance at elevated temperatures. These properties make TZM alloy a candidate material for tooling die in electric field sintering techniques (FAST). FAST is a recently developed technique for multimaterial complex shape component manufacturing, including the production of parts of small sizes and complex geometries [1]. Applying heat by external electric current, the plasticity induced in the sintered material (also called electroplasticity) paves the way [2], to enable the forming of difficult-to-process materials such as titanium alloys and hard ceramics. FAST process is particularly suitable for mass production of miniature or micro-parts due to its rapid heating nature as described in the literature [2].

Today, graphite is the most used material for FAST tool dies, due to its mechanical stability at high temperatures; required to be up to 800-900 ºC for metal powders and up to 1300 ºC for ceramic powder sintering. However, graphite is brittle and difficult to machine. Given that the FAST tool dies should withstand pressures of up to 150 MPa, under high temperatures [3], TZM seems an appropriate alternative tool material for this specific application. However, TZM alloy shows poor oxidation resistance at temperatures above 400 ºC [4]. In this case, when the size of the tools and components is scaled down to millimetres, soldering due to severe adhesion between the mould and the working material would occur and therefore, the demoulding may become a major challenge. For this reason, and as a part of the EU research project FP7-MicroFast-608720, this work focuses on the investigation of high oxidation protection coatings to enable the use of this alloy in FAST processes, specifically those deposited by vacuum physical vapour deposition (PVD) techniques [5], [6].

High oxidation resistance coatings deposited by PVD or CVD techniques have been extensively investigated in the literature [7]–[9]. Chromium or titanium nitrides containing either Al (ternary) or Al and Si (quaternary) have demonstrated excellent thermal stability and oxidation resistance at temperatures of up to 900 ºC [10]–[12]. Above these temperature ranges (i.e. 1000 ºC and higher) the coatings decompose under different mechanisms and evolve to oxides with different compositions and microstructures, thus experiencing volumetric changes which cause film structural failures due to cracking.

Cr-Al-O coating systems deposited by PVD have been investigated in the last decade as a coating material able to approach the mechanical performance α-Al_2O_3 phases [13], [14]. These coating can form solid solutions of the type α-$(Cr,Al)_2O_3$ for certain composition ranges at temperatures accessible by PVD techniques of 400-550 ºC [15], due to the fact that its precursors, α-Cr_2O_3 and α-Al_2O_3, crystallize in the same spatial group R-3c. On the other hand it has been reported that solid solutions of cubic fcc-$(CrAl)_2O_3$ lattice structure can also be formed and are mechanically valid for applications on cutting tools. Various scientific papers [16]–[21] have reported the composition, microstructure, lattice and mechanical/wear properties of Cr-Al-O and Cr-Al-O-N coating systems. Hirai et al. [22] reported on Cr-Al-O synthesized by pulsed laser deposition at a substrate temperature of 400 °C, obtaining fcc cubic structures and a metal non-metal ratio of 1 and an oxygen content of 25 at.%. Pedersen et al [15] and Diechle et al [23] reported the formation of corundum-like structures in DC and r.f. sputtered Cr-Al-O films.

Khatibi et al [18] studied the system $(Al_xCr_{1-x})_{2+y}O_{3-y}$ for various deposition conditions in cathodic arc evaporation. The corundum phase was favoured at high Cr content and at high O_2 flows, while the cubic phase was observed mostly for high Al content and

low O_2 flow. Diechle et at [23] found that the sputtered coatings developed corundum structures α-$(Al_{1-x},Cr_x)_2O_3$ in the form solid solutions. Najafi et al [24] found that the coatings Cr-Al-O could dynamically evolve from a fcc cubic crystalline structure to a α-$(CrAl)_2O_3$ during the deposition process when the coating thickness exceeded 2 microns. Ramm et al [25] developed different coating microstructures and compositions based on the pulsed electron emission P3e arc evaporation of Cr/Al cathodes in oxygen atmospheres. They showed that the produced coatings developed corundum-like lattice structure forming a solid solution of the type $(Al_{1-x}Cr_x)_2O_3$.

The thermal stability and oxidation resistance of Cr-Al-O coatings have also been addressed in different studies. Khatibi et al [18] showed that the thermal annealing of fcc-$(Al_{0.83}Cr_{0.17})_{2.3}O_{2.7}$ leads to the transformation from fcc to a corundum structure which initiates at 900 ºC and is totally completed at temperatures above 1000 ºC. In the case of films with an original corundum structure in the as deposited state, the thermal annealing did not lead to any structural modifications up to 1100 ºC. Similar results were found by Edlmayr et al [26] on vacuum annealed arc deposited coatings.

Even if the composition of a coating defines its performance, it only does it partially. Its structure or architecture design plays also an important role. Multilayered PVD coatings with different compositions provides the possibility to obtain enhanced hardness, toughness and thermal stability [27]. In this paper a CrAlO monolayer and a CrAlO/CrAlN multilayer PVD coatings have been studied as possible surface modification solutions to enable the use of TZM alloy in high temperature, >1000 ºC, FAST sintering. Most of the existing literature references reports on single coating structures [18], [23], [24] and their properties. Only one recent, to the best of our knowledge, reports on the properties of CrAlO/CrAlN nanomultilayers [28].

The "in service" performance of these substrate-coating systems was finally tested by the realization of sintering trials, and the corresponding visual inspection of the sintered parts and the coating integrity.

2. Experimental

2.1 Coating deposition

The coatings have been produced by cathodic arc evaporation in a commercial METAPLAS MZR-323 PVD reactor. The reactor is equipped with 2 opposing evaporation panels, each of them hosting 3 circular cathodes (63 mm diameter) vertically aligned. The effective coating volume is about 400 mm × 400 mm × 500 mm. For the preparation of the coatings, cathodes of two types were used: cathodes of Cr (99.8 % purity) for the bonding layer and of CrAl (50 at.% Cr - 50 at.% Al) for the rest of the coating. All the relevant process parameters are depicted in Table 1.

Table 1: Experimental parameters of the deposition processes.

Coating	**Material**	**A·h**	**No. of bilayers**	**Gases**	**Total Pressure (Pa)**
Bonding layer	Cr	20	-	Ar	1.2
	CrN	40	-	N_2	1.8
Monolayer	CrAlON	100	-	N_2+O_2 (63:37)	1.8
Multilayer	CrAlON	50	5	N_2+O_2 (63:37)	1.8
	CrAlN	50		N_2	1.8

For the coating deposition, high purity Ar, N_2 and/or O_2 gases were introduced in the chamber. A continuous DC bias of -50 V was applied on the substrates during the

deposition process. During all the processes, the substrates were rotated around the central vertical axis of the reactor chamber at a speed of 5 rpm. A Cr+CrN adhesion layer was deposited for all the coatings. The deposition temperature of 470 °C for the monolayer process and 500 ºC for the multilayer process was achieved by a combined plasma and electrical resistance heating process. Process temperatures have been monitored using the tempering hardness–temperature curve of 100Cr6 steel, by putting hardened samples of this material in the vacuum chamber during all the processes as reported by Fernández de Ara et al. [29].

2.2 Substrate materials

Four different substrate materials were used for the study: 40 mm diameter discs of H13 hot work steel (53-54 HRc), with a chemical composition in weight of 0.40 % C, 1.2 % Si, 0.30 % Mn, 5.5 % Cr, 1.2 % Mo and 0.86% V; 40 mm diameter discs of Inconel 718 with a chemical composition in weight of 51.7 % (Ni+Co), 19.7 % Cr, 4.8 % (Nb+Ta), 3.1 % Mo, 1.0 % Ti, 0.40 % Al; punches of Titanium-Zirconium-Molybdenum (TZM) alloy with a chemical composition of 0.50 % Ti, 0.08 % Zr, 0.02 % C and Mo (balance); and Boron doped Si wafers with a thickness of 525 ± 15 µm from Si-Mat. Discs of H13 steel and of Inconel 718 were mirror polished (Ra < 15 nm) and cleaned in ultrasonic bath using de-oiling agents and de-ionised water. All the substrates were vacuum-heated and ion-bombarded before the coating process.

2.3 Characterization techniques

Glow Discharge Optical Emission Spectroscopy (GDOES) was used to obtain the chemical composition depth profiles of the films. The GDOES analyses were done in a Jovin-Yvon JY 1000 RF optical spectrometer equipped with 40 detection channels. Glancing incidence X-ray diffraction (GI-XRD) diffractograms of the coatings were acquired in a D8 Advance Bruker diffractometer using a Cr $K\alpha_1$ radiation source (λ = 0.22897 nm) at an incidence angle of 1º. The coating thickness was measured with the help of the Calotest (CSM instruments, ball diameter 30 mm). The surface roughness was measured before and after coating deposition with a WYCO-RST 500 white light profilometer using the vertical scanning interferometry mode (VSI). For the wear resistance analysis, CSM HT tribometer under ball-on-disc configuration was used. The sliding tests were made using alumina counterballs of 6 mm in diameter at normal loads of 5 N when carried out at room temperature and at 2 N when carried out at high temperature (200 ºC and 400 ºC). The wear rates were calculated after measuring the volume losses of the specimens by white light profilometry. A Field Emission Scanning Electron Microscope (FESEM) HITACHI S-4800, coupled with an Energy Dispersive X-ray Spectroscopy (EDX) detector for elemental analysis, was used to inspect the cross section of the films.

Nanoindentation tests were performed on as-deposited samples using a Hysitron Triboindenter© 950 fitted with a Berkovich indenter with a tip end radius of around 150 nm. Forty indentations, separated enough between them not to influence each other, were made on the samples at 5 mN of maximum load. The load function consisted on 5 seconds of loading segment, followed by 2 seconds of holding time to account for material creep and 5 seconds of unloading.

The Oliver and Pharr method [30] was used to extract the hardness and Young's modulus values from the curves. At 5 mN, the maximum penetration of the indenter in the surface was around 120 nm for a 1.8 μm thick for the monolayer coating, and around 105 nm for a 2.4 μm thick multilayer coating. Those penetrations are well below the 10 % of the total thickness of the coating, value widely accepted for the measuring of the mechanical properties of the layer with no interference of the substrate.

High temperature annealing tests in ambient air were carried out in a Nabertherm LT 24/11/B180 muffle oven from 800 ºC up to 1100 ºC in steps of 100 ºC. A heating rate of 20 $^{o}C \cdot min^{-1}$, a holding time of 2 hours was used for each step sample and natural oven cooling. Nanoindentation tests and SEM-EDX analyses were carried out after the high temperature annealing tests.

2.4 Sintering trials

A Gleeble-3800 thermal simulation machine was used for the Micro-FAST sintering tests of Al_2O_3 (99.9% purity) and Ti90Sn10 (99.9%) powders with averaged particle size of 0.18 μm and 10-45 μm respectively were used for the sintering experiments. The powders were synthesized by high energy ball milling at MBN nanomaterialia S.r.l. The tooling rig consists of a TZM punch / graphite die couple, as shown in Figure 5. Two TZM punches, coated with a commercial PVD CrAlSiN and PVD AlCrO/AlCrN multilayer respectively were prepared for the sintering of a cylindrical sample of Φ4.0 mm × 4.0mm aiming to examine the feasibility of the PVD coating on TZM punch. The deposition conditions and properties of the CrAlSiN PVD coating are described by R. Ji [31] and dimensions of the die and punches by Hijji et al. [2]. The pre-determined

amount of powders were poured into the graphite die and then closed by the pre-coated TZM punch. A heating rate of 50 °C/s and a holding time of 240 s were used to sinter the powders under a pressure of 75 MPa in vacuum (45 Pa). Two sintering temperatures of 900 °C and 1100 °C were used for Ti90Sn10 powders and of 1200 °C and 1300 °C for Al_2O_3 powders.

3. Results and discussion

3.1 Chemical composition and microstructure

Figure 1 shows the chemical in-depth profiles of both coatings obtained by GD-OES.

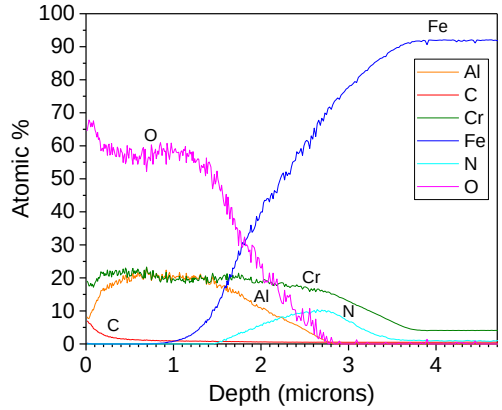

a)

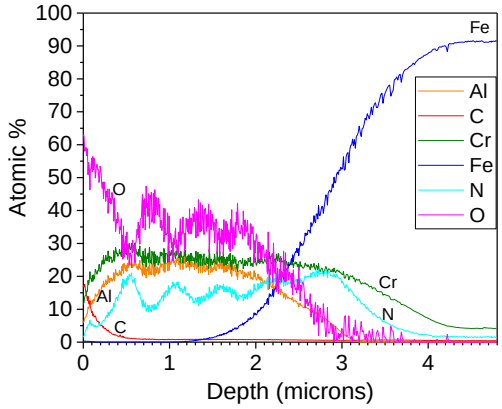

b)

Figure 1: GD-OES analyses of the a) monolayer CrAlO coating, and b) multilayer CrAlO/CrAlN coating.

Both coatings present a Cr/Al atomic ratio close to 1/1, in agreement with the nominal composition of the cathodes. In the case of the monolayer, the overall chemical composition responds to the stoichiometric formula $(Cr,Al)_2O_3$. In the case of the multilayer the alternation of the oxide and the nitride coatings hinders a totally reliable quantification of the composition for the individual sub-layers. In any case, it can be seen that the nitrogen composition of the nitride sublayers is smaller than the sum of the Cr plus Al. On the other hand, the oxide sublayers seem to retain the chemical composition of the corresponding monolayer, as the deposition conditions are similar in both cases. The total thicknesses of the monolayer and the multilayer coatings on H13

were 1.8 microns and 2.4 microns respectively. The difference in thickness is due to a higher coating growth speed of the nitride sublayers than that of the oxides, as reported by Khatibi et al [32]. The bilayer period of the multilayer (λ) is of 250 nm on silicon substrate and the thickness ratio of the CrAlO/CrAlN is approximately 2:1.

Figure 2 show the cross-section images of the coatings as deposited on Si substrates (the silicon substrate appears darker than the coating). The Cr+CrN bonding layer, of around 200 nm, can be clearly distinguished.

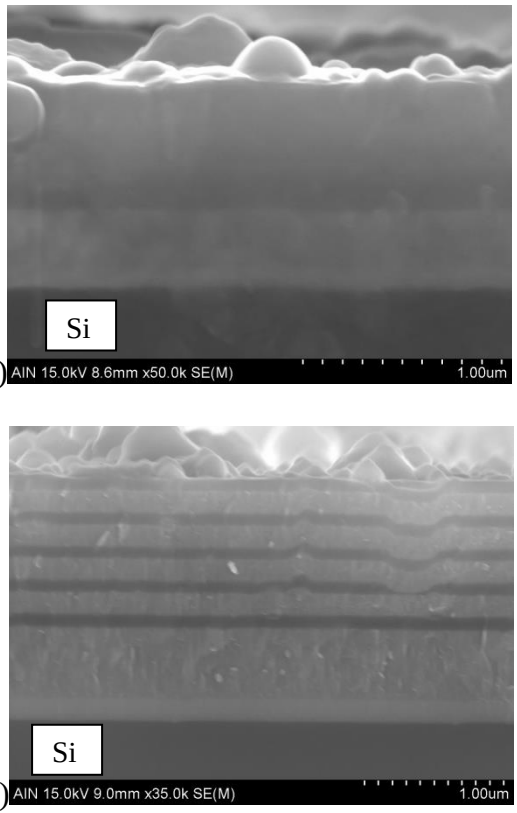

Figure 2: SEM images of the cross-section of as-deposited coatings on Si waflers, a) monolayer CrAlO, b) multilayer CrAlO/CrAlN.

The monolayer presents a compact structure in which some columnar growth can be distinguished. On the other hand the multilayer exhibits a dense columnar structure in the nitride layer (bright), which is barely replicated in the oxide sublayers (dark). The monolayer coatings in general exhibit a higher number of internal droplets than the multilayer. This excess of droplets is caused by the poisoning of the Cr/Al in the presence of oxygen.

Figure **3** shows the diffractograms of the deposited coatings on Inconel substrates.

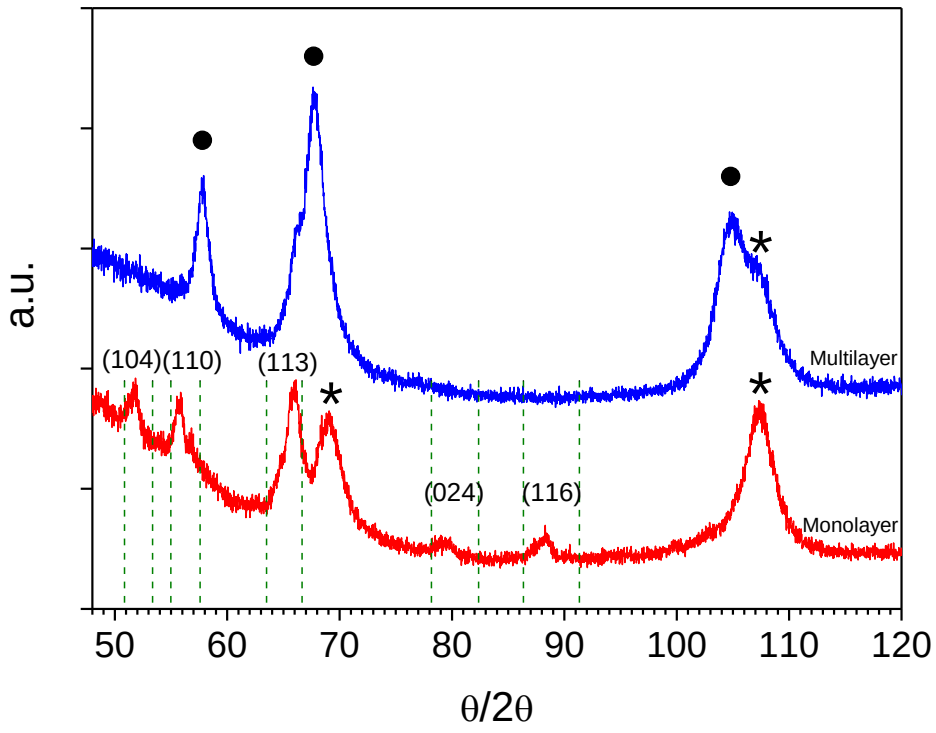

Figure 3: GI-XRD diffractograms of both untreated coatings.

The diffractogram of the monolayer coating shows peaks centered at 51.8º, 55.8º, 65.9º, 79.3º and 88.4º, which are all located in between the theoretical positions of the planes (104), (110), (113), (024) and (116) respectively, of the phases α-Cr_2O_3 eskolaite and α-Al_2O_3 corundum, (lower and upper limits in 2θ indicated as green dotted lines). This group of peaks exhibits large widths, indicating the presence of small size crystalline domains. No double peaks are observed in this set of diffractions, which may indicate the formation of a lattice structure of the 'solid solution' type. At the 2θ range where the plane (113) of eskolaite-corundum diffracts, there are also other possible contributions giving rise to reflections such as AlCr intermetallics. Therefore, the peak at 65.9º cannot be invariably assigned to the plane α-(113).

The peak at 69.1º, marked with an asterisk, can be attributed to a diffraction of a lattice plane (002) of a cubic fcc phase, likely of $(Cr,Al)_2O_3$ stoichiometry, as shown by GDOES. This is compatible with Khatibi et al [18] and more recently by different authors [24], who observed the presence of cubic fcc lattice structures in arc deposited coatings of stoichiometry close to $(Cr,Al)_2O_3$. This phase has been described as a cubic fcc lattice with a 33% cation vacancies. The corresponding lattice parameter obtained using the Bragg equation and the miller indexes (200) is 0.402 nm, close to that found by Khatibi et al. [33] for the cubic fcc lattice phases (0.404 nm) of stoichiometry $(Cr_xAl_{1-x})_2O_3$ with $0.6 < x < 0.7$. On the other hand, the peak at 107.3º is compatible with the reflections of the planes (022) of the same cubic structure. In fact, the estimated lattice parameter using the miller indexes (022) is also of 0.402 nm.

The diffraction pattern of the CrAlO/CrAlN multilayer exhibits mainly the reflections of the planes (111), (200) and (022) of the fcc CrAlN at 57.8º, 67.7º and 104.8º, which appear in Figure 3 marked with a black circle. This is in agreement with the larger volume fraction of nitride sub-layers with respect to the total film volume, as observed

by SEM cross sections. On the other hand the diffraction pattern of the multilayer sample also exhibits diffraction peaks at 65.9º, from the (113) planes of the α-$(Cr,Al)_2O_3$ phase and at 107.3º attributed to the (022) planes of the cubic fcc-$(Cr,Al)_2O_3$, in the form of shoulders of the (200) and (022) fcc-CrAlN peaks respectively. These peaks stem from the oxide sublayers of the multilayer. None of the other peaks present in the monolayer coating could be observed in the multilayer formulation.

3.2 Roughness, hardness and wear tests

Table 2 shows the roughness (Ra: arithmetic average height in the profile and Rq: geometric average height in the profile) and thickness of the coatings. The roughness values of the monolayer are higher than these typically obtained for transition metal nitrides deposited by CAE-PVD as in the cases of Antonov et al [34] and Bayón et al [35] where they obtained Ra roughness values in the range of the 30 to 100 nm.

Table 2: Roughness (Ra and Rq) and thickness of the monolayer and multilayer coatings.

Coating	Ra (nm)	Rq (nm)	Coating thickness (µm)
Monolayer	135.2 ± 15.9	231.8 ± 33.1	1.8 ± 0.1
Multilayer	58.2 ± 2.6	120.8 ± 9.2	2.4 ± 0.2

This is due to the presence of oxygen in the chamber during the deposition. This fact was also reported by Khatibi et al. [32] and Sjölén et al. [36], who found that the introduction of O_2 in the chamber as a reactive gas results in the extension of arcs over the target surface compared to the locally dense arcs formed in a pure nitrogen atmosphere. On the contrary, the roughness values of the multilayer coating are significantly smaller than these of the monolayer (cf. Table 2), due to the absence of oxygen gas during the nitride deposition cycles. During these cycles, the oxide layer of the target is removed, leading to a lesser ejection of microdroplets.

Table 3 shows the indentation hardness and modulus of the coatings, as deposited and after a thermal annealing in air at 1000 ºC for the monolayer; and 1000 ºC and 1100 ºC in the case of the multilayer. The multilayer coating exhibits an indentation hardness of 29.8 GPa and a modulus of 219 GPa; whereas these for the monolayer are 25.2 GPa and 193 GPa respectively. Different values of indentation hardness are reported in the literature for Cr-Al-N, Cr-Al-O and a multilayer CrAlO/CrAlN [28]. Arc evaporated CrAlN and CrAlSiN hardness as high as 35-40 GPa has been reported by Endrino et al [37] and Polcar et al [38]. Khatibi et al [18] reported values from 24 to 30 GPa for arc deposited CrAlO films depending on the Cr/Al ration, and Najafi et al [21] in the range 33 to 25 GPa. Cr-Al-O sputtered coatings, on the other hand, exhibited hardness between 24–27 GPa [15]. Raab et. al [28] found that the indentation hardness of CrAlO/CrAlN multilayers as the bilayer period increases. The hardness/modulus ratio H^3/E'^2 has also been calculated for the two coatings, as an indicator of the resistance to plastic deformation [38]. In this case, the H^3/E'^2 of the multilayer coating is higher than that of the monolayer.

Table 3: Hardness, Young Modulus and H^3/E'^2 values of the CrAlO monolayer coating and of the CrAlO/CrAlN multialyer coating in the untreated state and after the high temperature resistance tests at 1000 ºC and 1100 ºC.

Coating	**Monolayer**		**Multilayer**		
State	As deposited	After annealing 1000 ºC	As deposited	After annealing 1000 ºC	After annealing 1100 ºC
H (GPa)	25.2 ± 2.7	25.8 ± 3.4	29.8 ± 2.6	27.9 ± 3.8	21.3 ± 3.6
E' (GPa)	193 ± 13	191 ± 13	219 ± 8	207 ± 20	194 ± 9
H^3/E'^2	0.430	0.471	0.552	0.507	0.257

Table 4: Wear rate (in units of m^3/Nm) at room temperature, 200 ºC and 400 ºC.

Sample	**Room temperature**	**200 ºC**	**400 ºC**
Monolayer	$(1.85 \pm 0.52) \times 10^{-16}$	$(7.39 \pm 1.10) \times 10^{-15}$	Catastrophic wear
Multilayer	$(3.45 \pm 1.30) \times 10^{-17}$	No measurable wear or build-up	No measurable wear or build-up

Table 4 shows the wear rates of the coatings measured at RT, 200 ºC and 400 ºC. At RT the monolayer coating shows a wear rate of 1.85×10^{-16} m^3/Nm, and the multilayer of 3.45×10^{-17} m^3/Nm, which is one order of magnitude smaller than that of the monolayer. At 200 ºC, the wear resistance of the monolayer coating decreases down to 7.39×10^{-15} m^3/Nm (cf. Table 4), and is strongly worsened at 400 ºC. The multilayer coating shows better wear resistance at 200 ºC and 400 ºC than at room temperature. Instead of revealing a wear track during the wear tests, a slight material growth could be

observed in the tracks. Polcar et al [38] showed values of wear rate for arc deposited AlCrN, and AlCrSiN films of around 5×10^{-16} m^3/Nm, well stable between RT and 400ºC, using similar testing conditions of 5N load with an Al_2O_3, 6 mm diameter counterball.

3.3 High temperature annealing tests

The morphology of the films after the annealing is shown in Figure 4 in plain view.

Temperature (ºC)	Monolayer	Multilayer
As deposited	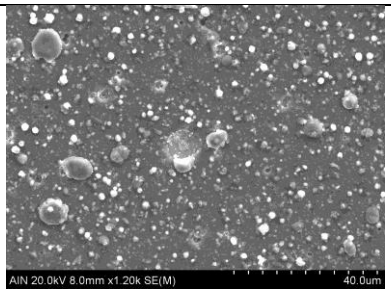	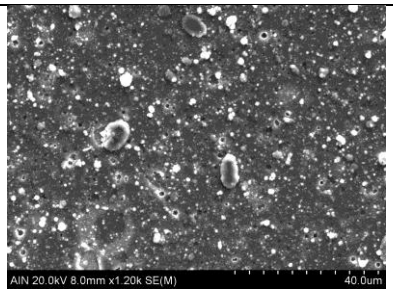
800	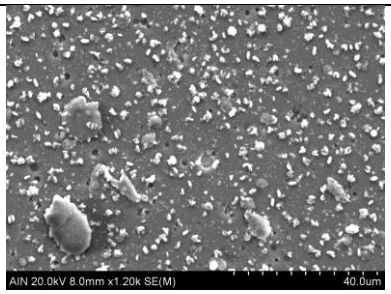	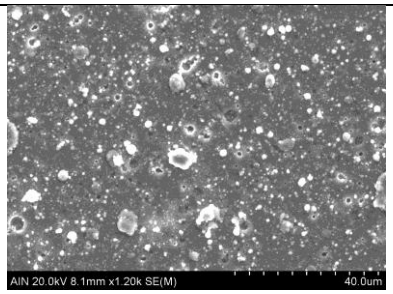
1000	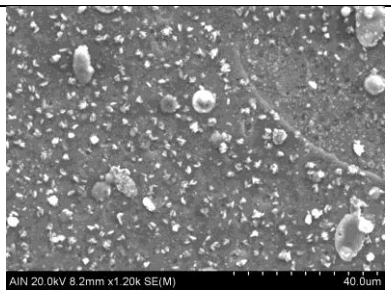	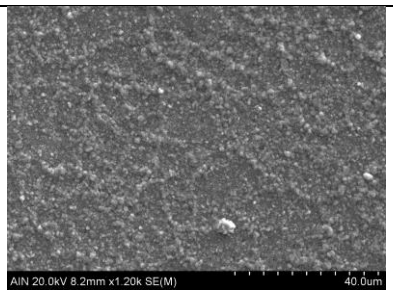

1100	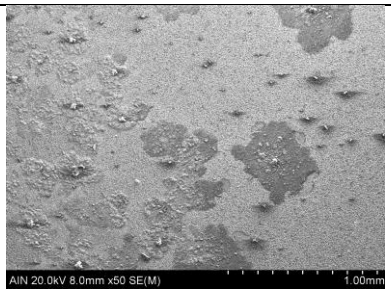	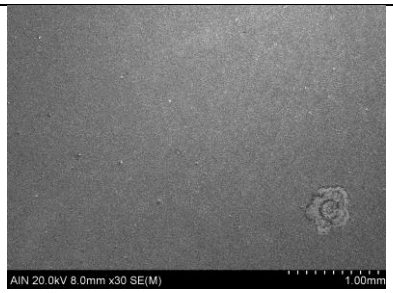
1100 higher magnification	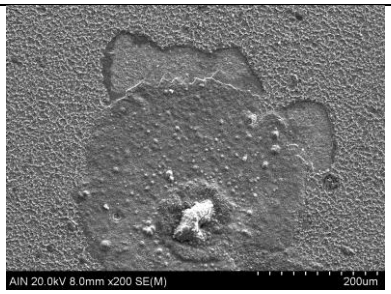	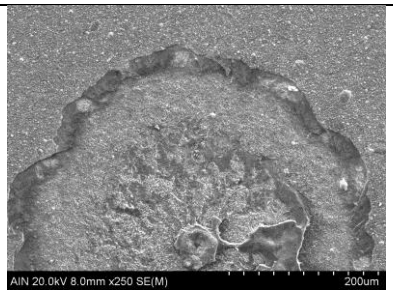

Figure 4: SEM images of the samples' surface untreated and after high temperature annealing tests.

In the range of 800 ºC to 1000 ºC, the samples showed features similar to those in the untreated state, and no major degradation signs could be observed in this temperature range. Annealing at 1100 ºC produced a transformation on the surface morphology of both coatings. The surface of the monolayer shows a large number of patches indicating a partial degradation of its integrity. In the case of the multilayered coating, the signs of thermal degradation are much less visible.

EDX semi-quantitative analyses have been done in different zones, and shown in Table 5, to confirm the coating detachment from the observed patches of Fig. 4 after annealing. In the insert of Table 5, the SEM plain view pictures of the patches for the monolayer and the multilayer is shown. *Zones 1*, correspond to the areas where the coating integrity is preserved, and *Zones 2* where the bare substrate is visible. The Ni, Fe and other element signals, from the substrate, increases in *Zones 2* with respect to

these measured on Zones 1, whereas the signal of the coating constituents, such as Cr, and Al decrease, though do not totally vanished.

Table 5: Semi-quantitative elemental analysis on the surface of the monolayer and the multilayer coated Inconel after annealing of 1100 ºC in air. Data in at%.

Monolayer		**Zone 1**	**Zone 2**
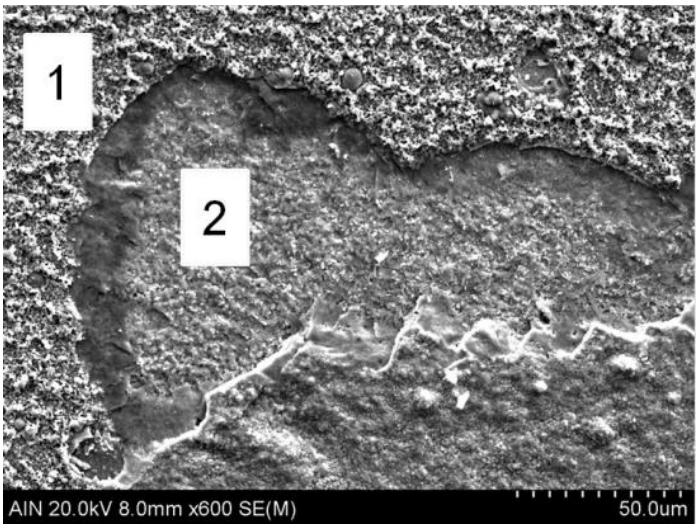	**N**	-	-
	O	63.83	57.75
	Al	4.26	1.50
	Ti	2.25	1.80
	Cr	28.74	11.78
	Mn	0.31	0.08
	Fe	0.31	3.84
	Ni	0.00	9.83
	Nb	0.30	13.41
Multilayer		**Zone 1**	**Zone 2**
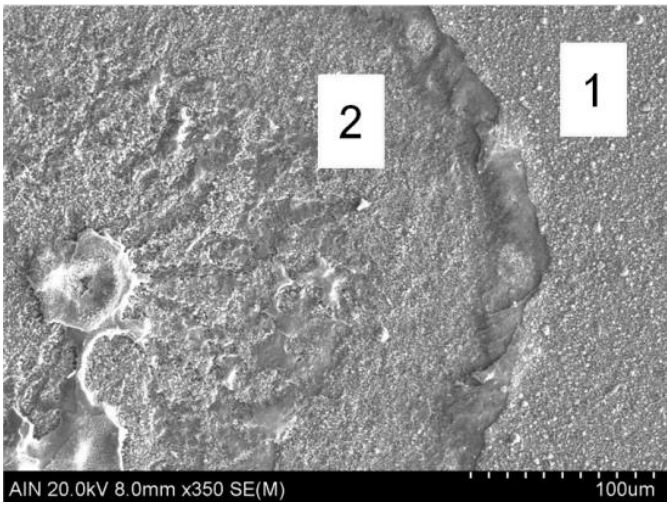	**N**	-	-
	O	52.59	69.32
	Al	5.03	4.21
	Ti	1.47	0.43
	Cr	37.32	15.51
	Mn	-	-
	Fe	1.10	0.94
	Ni	2.49	6.62
	Nb	0.00	2.96

With regards to the mechanical properties after annealing, the hardness of the annealed monolayer coating (cf. Table **3**) remains at the same value at 1000 ºC as this measured at RT, whereas the hardness of the multilayer slightly decreases to 27.9 GPa. After the annealing at 1100 ºC the monolayer coating is not stable anymore and the nanoindentation curves do not provide reliable hardness values. Interestingly the multilayer coating shows a high stable hardness value of 21.3 GPa even after an annealing at 1100 ºC. The mechanical stability of Cr-Al-O coatings has also been reported by only few authors. For example, Khatibi et al. [18] reported that the indentation hardness of arc evaporated Cr-Al-O coatings dropped 3 - 5 GPa after annealing at 1100 °C compared with the untreated in the fcc cubic state. Tien et al [39], reported on the decrease of CrAlSiN arc deposited coatings from 30.2GPa to 28.3 GPa after 1 h thermal annealing at 900ºC. At 1100ºC, the degradation of the coating hindered reliable measurements of indentation hardness.

3.4 Sintering trials

For the FAST sintering trials, the multilayer coating performance has been qualitatively compared with a benchmark CrAlSiN coating deposited by arc evaporation. It is noteworthy to highlight that, with the bare TZM punch uncoated, the sintering trials were unsuccessful because the powders stuck on the tool, making the part ejection not possible.

Figure 5 shows the graphite die and the TZM punch after sintering of *a)* Ti90Sn10 powders at 1100 ºC and *b)* Al_2O_3 powders at 1300 ºC. After sintering Ti90Sn10 powders at temperature of 900 °C and 1100 °C, the TZM punch coated with the

CrAlSiN benchmark coating can be easily withdrawn from the graphite die without sticking. The TZM punch coated with CrAlO/CrAlN coating can be also slipped out of the die and the sintered Ti90Sn10 part, with a relative density of 95 %, could be easily separated from the punch (Figure 5a).


a)

b)

Figure 5: PVD coated TZM punches and graphite die assembly after sintering a) Ti90Sn10 powders at 1100 ºC and b) Al_2O_3 powders at 1300 ºC. The punch on the left of both photos is CrAlO/CrAlN coated and the one in the right CrAlSiN coated.

The PVD coated TZM punches / graphite die assemblies were further tested by sintering Al_2O_3 powders at 1200 °C and 1300 °C (Figure 5b). After the sintering, the TZM punch with the CrAlO/CrAlN coating can be easily pulled out of the graphite die without sticking. The sintered Al_2O_3 sample has a relative density over 90 % and it could be ejected out of the graphite die by standard procedures. After four Al_2O_3 powder sintering tests, the punches were sectioned to inspect the integrity of the coatings. The TZM punch coated with CrAlSiN coating can be taken off the die but the punch surface became rougher indicating that the CrAlSiN coating was degraded at such high temperatures. As observed in Figure 6a, some Al_2O_3 and graphite debris remained stuck on the surface of the CrAlSiN coated TZM punch, which could be confirmed by the EDX analysis, and the coating was partially damaged after sintering Al_2O_3 powders at 1300 °C.

a) 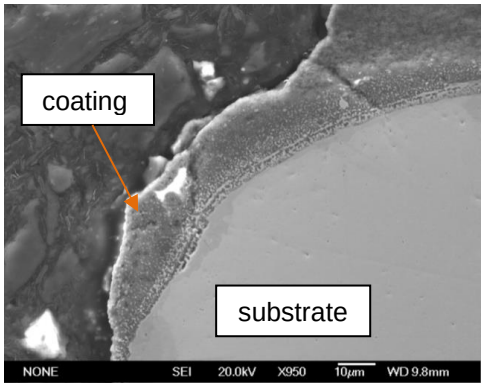

b) 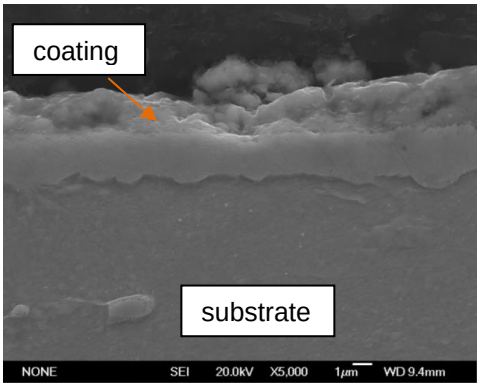

Figure 6: Cutaway views of the TZM punches after 4 sinterings a) CrAlSiN coated and b) CrAlO/CrAlN coated.

On the other hand, the amount of adhered Al_2O_3 sintered powders on the punch coated with the multilayer is much smaller, as shown in Figure 6b; in addition the integrity of the CrAlO/CrAlN multilayer coating on the TZM punch is mostly preserved after 4 sintering cycles.

All the observed results indicate that the multilayering structure of the CrAlO/CrAlN coating system produces a superior mechanical and tribological performance over the CrAlO at room and at high temperatures. In fact the benefit of multilayering has been well reported in the literature [40-43]. The presence of various dissimilar material interfaces in a coating system can block the propagation of cracks at the interface of the tougher part [40]. The alternation of two different layer also forces the re-nucleation during the film growth allowing to obtain more dense and compact growth [42]. The multilayering is an effective strategy for the blockage of pinholes formation through to the substrate [43], thus hindering the oxidation kinetics and the consequent degradation of the coatings and substrate system [42].

4. Conclusions

Monolayer CrAlO and multilayer CrAlO/CrAlN coatings have been deposited by industrial-scale cathodic arc evaporation system in N_2/O_2 atmosphere. The CrAlO exhibited an undetermined volume fraction mixture of cubic and corundum phases of stoichiometry close to $(Cr,Al)_2O_3$. The multilayer showed the prevalence of the cubic structure of the CrAlN and some volume fractions of the cubic and corundum oxide phases from the oxide sublayers. The structural, mechanical and tribological results evidence a strong dependence on the film structure. The multilayer CrAlO/CrAlN coating exhibited higher mechanical stability after thermal annealing at 1000ºC and 1100ºC than these of the monolayer. The multilayer retained the high hardness up to 1100ºC of annealing, whereas it did not show hints of structural degradation until 1100ºC. In addition, the multilayer has been also shown to enhance wear resistance performance of the monolayer CrAlO at RT and at 400ºC.

In the sintering trials, both CrAlSiN monolayer and CrAlO/CrAlN multilayer coating have been proved to be adequate to coat punches used for the sintering of Ti90Sn10 allowed powders. On the other hand, the CrAlO/CrAlN multilayer coating qualitatively showed protection properties to the TZM punch tool during the sintering of Al_2O_3, with respect to that show by the CrAlSiN coating.

Acknowledgements

We acknowledge the financial support of the European Commission through the FP7 Grant Agreement 608720 (Micro-FAST), and the MINECO (Spain) in the frame of the PROTEOX project (MAT2013-45391-P). The authors want to thank Alberto Colella and Prof. P. Matteazzi from MBN nanomaterialia S.r.l. for the supply of the Ti90Sn10 and Al_2O_3 powders.

References

[1] D. Lu, Y. Yang, Y. Qin, and G. Yang, "Forming microgears by micro-FAST technology," *J. Microelectromechanical Syst.*, vol. 22, no. 3, pp. 708–715, 2013.

[2] H. Hijji, Y. Qin, K. Huang, M. Bin Zulkipli, S. Yang, and J. Zhao, "Forming alumina (Al_2O_3) by micro-FAST," in *Advances in Manufacturing Technology XXX*, Y. M. Goh and K. Case, Eds. 2016, pp. 61–66.

[3] Z. A. Munir, D. V. Quach, and M. Ohyanagi, "Electric current activation of sintering: A review of the pulsed electric current sintering process," *Journal of the American Ceramic Society*, vol. 94, no. 1. pp. 1–19, 2011.

[4] M. E. Cura *et al.*, "Friction behavior of alumina/molybdenum composites and formation of MoO_{3-x} phase at 400 ºC," *Tribol. Int.*, vol. 87, pp. 23–31, 2015.

[5] S. P. Chakraborty, S. Banerjee, K. Singh, I. G. Sharma, A. K. Grover, and A. K. Suri, "Studies on the development of protective coating on TZM alloy and its subsequent characterization," *J. Mater. Process. Technol.*, vol. 207, no. 1–3, pp. 240–247, 2008.

[6] Z. Zhang, X. Li, E. Almandoz, G. G. Fuentes, and H. Dong, "Sliding friction and wear behaviour of Titanium-Zirconium-Molybdenum (TZM) alloy against Al_2O_3 and Si_3N_4 balls under several environments and temperatures," *Tribol. Int.*, vol. 110, 2017.

[7] J. Lin, J. J. Moore, J. Wang, and W. D. Sproul, "High temperature oxidation behavior of CrN/AlN superlattice films," *Thin Solid Films*, vol. 519, no. 8, pp. 2402–2408, 2011.

[8] J. Musil, "Hard nanocomposite coatings: Thermal stability, oxidation resistance and toughness," *Surf. Coatings Technol.*, vol. 207, pp. 50–65, 2012.

[9] Y. P. Feng, L. Zhang, R. X. Ke, Q. L. Wan, Z. Wang, and Z. H. Lu, "Thermal

stability and oxidation behavior of AlTiN, AlCrN and AlCrSiWN coatings," *Int. J. Refract. Met. Hard Mater.*, vol. 43, pp. 241–249, 2014.

[10] M. Witthaut, R. Cremer, A. von Richthofen, and D. Neuschütz, "Improvement of the oxidation behavior of $Ti_{1-x}Al_xN$ hard coatings by optimization of the Ti/Al ratio," *Fresenius. J. Anal. Chem.*, vol. 361, no. 6, pp. 639–641, 1998.

[11] Y. C. Chim, X. Z. Ding, X. T. Zeng, and S. Zhang, "Oxidation resistance of TiN, CrN, TiAlN and CrAlN coatings deposited by lateral rotating cathode arc," *Thin Solid Films*, vol. 517, no. 17, pp. 4845–4849, 2009.

[12] D. Chaliampalias *et al.*, "Compositionally gradient PVD CrAlSiN films: structural examination and oxidation resistance," *Surf. Eng.*, vol. 844, no. July, pp. 1–7, 2016.

[13] K. Bobzin, "High-performance coatings for cutting tools," *CIRP J. Manuf. Sci. Technol.*, no. 2016, 2016.

[14] B. P. Dhonge *et al.*, "Wear and oxidation resistance of combustion CVD grown alumina films," *Surf. Coatings Technol.*, vol. 206, no. 22, pp. 4574–4579, 2012.

[15] K. Pedersen, J. Bøttiger, M. Sridharan, M. Sillassen, and P. Eklund, "Texture and microstructure of Cr_2O_3 and $(Cr,Al)_2O_3$ thin films deposited by reactive inductively coupled plasma magnetron sputtering," *Thin Solid Films*, vol. 518, no. 15, pp. 4294–4298, 2010.

[16] L. de Abreu Vieira *et al.*, "Approaches to influence the microstructure and the properties of Al-Cr-O layers synthesized by cathodic arc evaporation," *Surf. Coatings Technol.*, vol. 204, no. 11, pp. 1722–1728, 2010.

[17] M. Pohler, R. Franz, J. Ramm, P. Polcik, and C. Mitterer, "Cathodic arc deposition of $(Al,Cr)_2O_3$: Macroparticles and cathode surface modifications," *Surf. Coatings Technol.*, vol. 206, no. 6, pp. 1454–1460, 2011.

[18] A. Khatibi, A. Genvad, E. Göthelid, J. Jensen, P. Eklund, and L. Hultman, "Structural and mechanical properties of corundum and cubic $(Al_xCr_{1-x})_{2+y}O_{3-y}$ coatings grown by reactive cathodic arc evaporation in as-deposited and annealed states," *Acta Mater.*, vol. 61, no. 13, pp. 4811–4822, 2013.

[19] M. Pohler, R. Franz, J. Ramm, P. Polcik, and C. Mitterer, "Influence of pulsed bias duty cycle variations on structural and mechanical properties of arc evaporated $(Al,Cr)_2O_3$ coatings," *Surf. Coatings Technol.*, vol. 282, pp. 43–51, 2015.

[20] J. Nohava, P. Dessarzin, P. Karvankova, and M. Morstein, "Characterization of tribological behavior and wear mechanisms of novel oxynitride PVD coatings designed for applications at high temperatures," *Tribol. Int.*, vol. 81, pp. 231–239, 2015.

[21] H. Najafi, A. Karimi, P. Dessarzin, and M. Morstein, "Correlation between anionic substitution and structural properties in $AlCr(O_xN_{1-x})$ coatings deposited by lateral rotating cathode arc PVD," *Thin Solid Films*, vol. 520, no. 5, pp. 1597–1602, 2011.

[22] M. Hirai, H. Saito, T. Suzuki, H. Suematsu, W. Jiang, and K. Yatsui, "Oxidation behavior of Cr-Al-N-O thin films prepared by pulsed laser deposition," in *Thin Solid Films*, 2002, vol. 407, no. 1–2, pp. 122–125.

[23] D. Diechle, M. Stueber, H. Leiste, S. Ulrich, and V. Schier, "Combinatorial approach to the growth of alpha-$(Al_{1-x},Cr_x)_2O_3$ solid solution strengthened thin films by reactive r.f. magnetron sputtering," *Surf. Coatings Technol.*, vol. 204, no. 20, pp. 3258–3264, 2010.

[24] H. Najafi, A. Karimi, P. Dessarzin, and M. Morstein, "Formation of cubic structured $(Al_{1-x}Cr_x)_{2+\delta}O_3$ and its dynamic transition to corundum phase during

cathodic arc evaporation," *Surf. Coatings Technol.*, vol. 214, pp. 46–52, 2013.

[25] J. Ramm, M. Ante, T. Bachmann, B. Widrig, H. Brändle, and M. Döbeli, "Pulse enhanced electron emission (P3e^{TM}) arc evaporation and the synthesis of wear resistant Al-Cr-O coatings in corundum structure," *Surf. Coatings Technol.*, vol. 202, no. 4–7, pp. 876–883, 2007.

[26] V. Edlmayr, M. Pohler, I. Letofsky-Papst, and C. Mitterer, "Microstructure and thermal stability of corundum-type $(Al_{0.5}Cr_{0.5})_2O_3$ solid solution coatings grown by cathodic arc evaporation," *Thin Solid Films*, vol. 534, pp. 373–379, 2013.

[27] U. Helmersson, S. Todorova, S. A. Barnett, J. E. Sundgren, L. C. Markert, and J. E. Greene, "Growth of single-crystal TiN/VN strained-layer superlattices with extremely high mechanical hardness," *J. Appl. Phys.*, vol. 62, no. 2, pp. 481–484, 1987.

[28] R. Raab, C. M. Koller, S. Kolozsvári, J. Ramm, and P. H. Mayrhofer, "Interfaces in arc evaporated Al-Cr-N/Al-Cr-O multilayers and their impact on hardness," *Surf. Coatings Technol.*, 324, pp. 236–242, 2017.

[29] J. Fernández de Ara, E. Almandoz, J. F. Palacio, G. G. Fuentes, R. J. Rodríguez, and J. A. García, "Influence of temperature in arc-activated plasma nitriding of maraging steel in solution annealed and aged conditions," *Surf. Coatings Technol.*, vol. 258, pp. 754–762, 2014.

[30] C. Oliver and M. Pharr, "An improved technique for determining hardness and elastic modulus using load and displacement sensing indentation experiments," *J. Mater. Res.*, vol. 7, no. 11, pp. 1564–1583, 1992.

[31] R. Ji, "Development and Characterisation of Nano-multilayer CrAlSiN Coating Systems for Cutting Tools."

[32] A. Khatibi, J. Sjölen, G. Greczynski, J. Jensen, P. Eklund, and L. Hultman,

"Structural and mechanical properties of Cr-Al-O-N thin films grown by cathodic arc deposition," *Acta Mater.*, vol. 60, no. 19, pp. 6494–6507, 2012.

[33] A. Khatibi *et al.*, "Face-centered cubic $(Al_{1-x}Cr_x)_2O_3$," *Thin Solid Films*, 519, pp. 2426–2429, 2011.

[34] M. Antonov, I. Hussainova, F. Sergejev, P. Kulu, and A. Gregor, "Assessment of gradient and nanogradient PVD coatings behaviour under erosive, abrasive and impact wear conditions," *Wear*, vol. 267, no. 5–8, pp. 898–906, 2009.

[35] R. Bayón *et al.*, "Corrosion-wear behaviour of PVD Cr/CrN multilayer coatings for gear applications," *Tribol. Int.*, vol. 42, no. 4, pp. 591–599, 2009.

[36] J. Sjölén, L. Karlsson, S. Braun, R. Murdey, A. Hörling, and L. Hultman, "Structure and mechanical properties of arc evaporated Ti-Al-O-N thin films," *Surf. Coatings Technol.*, vol. 201, no. 14, pp. 6392–6403, 2007.

[37] J. L. Endrino and V. Derflinger, "The influence of alloying elements on the phase stability and mechanical properties of AlCrN coatings," *Surf. Coatings Technol.*, vol. 200, no. 1–4 SPEC. ISS., pp. 988–992, 2005.

[38] Tomas Polcar, Albano Cavaleiro. High-temperature tribological properties of CrAlN, CrAlSiN and AlCrSiN coatings. Surface & Coatings Technology 206 (2011) 1244–1251

[39] Tien, S.-K., Lin, C.-H., Tsai, Y.-Z., Duh, J.-G. Microstructural evaluation of high oxidation resistant CrAlSiN hard coating at elevated temperature in air atmosphere. Key Engineering Materials. 373-374 (2008) 446-451

[40] J. Musil, F. Kunc, H. Zeman, and H. Poláková, "Relationships between hardness, Young's modulus and elastic recovery in hard nanocomposite coatings," *Surf. Coatings Technol.*, vol. 154, no. 2–3, pp. 304–313, 2002.

[41] C. H. R. V. Kumar, P. K. Nair, and B. Ramamoorthy, "Characterization of

multilayer pvd nanocoatings deposited on tungsten carbide cutting tools," *Int. J. Adv. Manuf. Technol.*, vol. 38, no. 5–6, pp. 622–629, 2008.

[42] H. Riedl, E. Aschauer, C. M. Koller, P. Polcik, M. Arndt, and P. H. Mayrhofer, "Ti-Al-N/Mo-Si-B multilayers: An architectural arrangement for high temperature oxidation resistant hard coatings," *Surf. Coatings Technol.*, vol. 328, pp. 80–88, 2017.

[43] W. Y. Ho, C. H. Shen, C. L. Chang, and D. Y. Wang, "Corrosion behaviors of Cr(N,O)/CrN multi-layered coatings by cathodic arc deposition," *Surf. Coatings Technol.*, vol. 202, no. 4–7, pp. 745–749, 2007.

Figure captions

Figure 1: GD-OES analyses of the a) monolayer CrAlO coating, and b) multilayer CrAlO/CrAlN coating.

Figure 2: SEM images of the cross-section of as-deposited coatings on Si waflers, a) monolayer CrAlO, b) multilayer CrAlO/CrAlN.

Figure 3: GI-XRD diffractograms of both untreated coatings.

Figure 4: SEM images of the samples' surface untreated and after high temperature annealing tests.

Figure 5: PVD coated TZM punches and graphite die assembly after sintering a) Ti90Sn10 powders at 1100 ºC and b) Al_2O_3 powders at 1300 ºC. The punch on the left of both photos is the CrAlO/CrAlN coated and the one in the right the CrAlSiN coated.

Figure 6: Cutaway views of the TZM punches after 4 sinterings a) CrAlSiN coated and b) CrAlO/CrAlN coated.

Table captions

Table 1: Experimental parameters of the deposition processes.

Table 2: Roughness (Ra and Rq) and thickness of the monolayer and multilayer coatings.

Table 3: Hardness, Young Modulus and H^3/E'^2 values of the CrAlO monolayer coating and of the CrAlO/CrAlN multilayer coating in the untreated state and after the high temperature resistance tests at 1000 and 1100 ºC.

Table 4: Wear rate (in m^3/Nm) at room temperature, 200 ºC and 400 ºC.

Table 5: EDX results on the surface of Inconel samples coated with the monolayer and the multilayer coatings affter the high temperature resistance tests at 1100 ºC.